DNS OF INCOMPRESSIBLE FLOWS USING LATTICE BOLTZMANN METHOD

NOBUYUKI SATOFUKA

Department of Mechanical and System Engineering,
Kyoto Institute of Technology,
Matsugasaki, Sakyou-ku, Kyoto 606-8585, JAPAN

Abstract

Numerical simulations using the lattice Boltzmann method are presented for the two- and three-dimensional decaying homogeneous isotropic turbulence for low, medium and high Reynolds numbers. Time history of global statistical quantities, wave number spectra, and vorticity contour plots are compared with those of the higher-order method of lines. Comparisons between the square lattice and the triangular (FHP) lattice models are also performed. It is found that the lattice Boltzmann method is able to reproduce the dynamics of decaying turbulence and could be an alternative for solving the Navier-Stokes equations. Computational costs of the lattice Boltzmann method is less than half of that of the 10th-order method of lines.

1. Introduction

The rapid development and introduction of new supercomputer systems over the last decade has opened new opportunities for numerical studies of incompressible fluid flows. The direct numerical simulations of turbulence is one of such problems. So far almost all direct simulations of turbulence has been carried out by either spectral[1] or pseudo spectral[2,3] approximation to spatial derivatives. However, these methods which require the use of series are global in character so that they are quite unsuitable for complex geometry problems and for parallel computing. Therefore, the development of more flexible and efficient methods is hoped for in the simulations of turbulence.

We have proposed a new higher-order method based on a method of lines (MOL) approach[4-7] and demonstrated that results obtained by the method were comparable to those using the pseudospectral method with less than one sixth of the computational time in direct simulation of two-dimensional homogeneous isotropic turbulence on 513×513 grid points.

In the later half of the 80's, a novel technique called Lattice Gas Automata (LGA) for solving the Navier-Stokes equations was developed. Since the first two-dimensional model representing incompressible Navier-Stokes equations was proposed by Frisch, Hasslacher, and Pomeau (FHP) in 1986[8], LGA have attracted much attention as promising methods for solving a variety of partial differential equations and modeling physical phenomena. The basic idea of LGA methods is to represent the fluid as an ensemble of interacting low-order bit-computers situated at regularly spaced lattice nodes. In the FHP model, the underlying lattice is a close-packed equilateral triangular lattice with nodes at triangle vertices, each node has a seven-bit state with the first bit specifying the existence or not of a particle at rest at the lattice node and the remaining six bits specifying the presence or not of a particle traveling at an angle $\vartheta_j = (\pi/3)j$ $(0 \leq j \leq 6)$ along the legs of the triangular lattice. Each particle (except a rest particle) moves one lattice distance in one fundamental time interval. After the particles propagate they then interact according to certain collision rules. Although the LGA method has provided a fast and efficient way for solving partial differential equations, there exist some fundamental problems in this method in simulating realistic fluid flows obeying the Navier-Stokes equations. Besides its intrinsic noisy character which makes the computational accuracy difficult to achieve, it contains certain properties even in the fluid limit. The lattice gas fluid momentum equations cannot be reduced to the Navier-Stokes equations because of two fundamental problems. The first is the non-Galilean invariance property due to the density dependence of the convection coefficient. This limits the validity of the LGA method only a strict incompressible region. Second the pressure has an explicit and unphysical velocity dependence. To avoid some of those inherent problems, several lattice Boltzmann (LB) models have been proposed[9-15]. The main feature of the LB method is to replace the particle occupation variables n_i (Boolean variables) by the single-particle distribution functions (real variables) $f_i = \langle n_i \rangle$, where $\langle\ \rangle$ denotes a local ensemble average, in the evolution equation, i.e., the lattice Boltzmann equation. The LB method as a numerical scheme was first proposed by McNamara and Zaretti[9]. In their model, the form of collision operator is the same as in the LGA, written in terms of distribution functions and completely neglecting the effect of correlations between particles. Higuera, Jimenez, and Succi[10,11] introduced a linearized collision operator that is a matrix and has no correspondence to

the detailed collision rules. Statistical noise is completely eliminated in both models; however, the other problems remain, since the equilibrium distribution is still Fermi-Diracs. The LB model proposed by Chen et al[12,13] and Qian et al[14,15] abandons Fermi-Dirac statistic and applies the single relaxation time approximation first introduced by Bhatnager, Gross, and Krook in 1954[16], to greatly simplify the collision operator. This model is called the lattice BGK (LBGK) model.

This paper organized as follows. In section 2 the lattice Boltzmann methods simulating the Navier-Stokes equations are discussed. The lattice Boltzmann simulation of two-dimensional homogeneous isotropic turbulence is presented in section 3. Three-dimensional homogeneous isotropic turbulence is presented in section 4. Accuracy and efficiency of the lattice Boltzmann method in comparison with the conventional higher-order MOL approach are also discussed. The final section contains concluding remarks.

2. Lattice Boltzmann Method

2.1. SQUARE LATTICE MODEL

In this section an outline is given of the LB methods with BGK model for the collision operator. A square lattice with unit spacing is used on which each node has eight nearest neighbors connected by eight links as shown in Fig.1. Particles can only reside on the nodes and move to their nearest neighbors along these links in the unit time. Hence, there are two types of moving particles. Particles of type 1 move along the axes with speed $|\mathbf{e}_{1,i}| = 1$ and particle of type 2 move along the diagonal directions with speed $|\mathbf{e}_{2,i}| = \sqrt{2}$. Rest particles with speed zero are also allowed at each node. The occupation of the three types of particles is represented by the single-particle distribution function, $f_{\sigma i}(\mathbf{x}, t)$, where subscripts σ and i indicate the type of particle and the velocity direction, respectively. When $\sigma = 0$, there is only f_{01}. The distribution function, $f_{\sigma i}(\mathbf{x}, t)$, is the probability of finding a particle at node $\mathbf{x}$ and time t with velocity $\mathbf{e}_{\sigma i}$. According to Bhatnagar, Gross, and Krook (BGK), the collision operator is simplified using the single time relaxation approximation. Hence, the lattice Boltzmann BGK (LBGK) equation (in lattice unit) is

$$f_{\sigma i}(\mathbf{x} + \mathbf{e}_{\sigma i}, t + 1) - f_{\sigma i}(\mathbf{x}, t) = -\frac{1}{\tau}[f_{\sigma i}(\mathbf{x}, t) - f_{\sigma i}^{(0)}(\mathbf{x}, t)] \qquad (1)$$

where $f_{\sigma i}^{(0)}(\mathbf{x}, t)$ is the equilibrium distribution at $\mathbf{x}, t$ and τ is the single relaxation time which controls the rate of approach to equilibrium. The density per node, ρ , and the macroscopic velocity, $\mathbf{u}$, are defined in terms of the particle distribution function by

$$\rho = \sum_{\sigma} \sum_{i} f_{\sigma i}, \quad \rho \mathbf{u} = \sum_{\sigma} \sum_{i} f_{\sigma i} \mathbf{e}_{\sigma i} \qquad (2)$$

A suitable equilibrium distribution can be chosen in the following form for particles of each type

$$f_{01}^{(0)} = \rho\alpha - \frac{2}{3}\rho\mathbf{u}^2 \tag{3}$$

$$f_{1i}^{(0)} = \rho\beta + \frac{1}{3}\rho(\mathbf{e}_{1i}\cdot\mathbf{u}) + \frac{1}{2}\rho(\mathbf{e}_{1i}\cdot\mathbf{u})^2 - \frac{1}{6}\rho\mathbf{u}^2 \tag{4}$$

$$f_{2i}^{(0)} = \rho\frac{(1-4\beta-\alpha)}{4} + \frac{1}{12}\rho(\mathbf{e}_{2i}\cdot\mathbf{u}) + \frac{1}{8}\rho(\mathbf{e}_{2i}\cdot\mathbf{u})^2 - \frac{1}{24}\rho\mathbf{u}^2 \tag{5}$$

The relaxation time is related to the viscosity by

$$\nu = \frac{2\tau-1}{6} \tag{6}$$

where ν is the kinematic viscosity measured in lattice units. In ref.[17], Hou et al used the value of $\alpha = 4/9$ and $\beta = 1/9$.

The equilibrium populations are determined by assuming that they can be expressed as a power series in velocity and density of the form:

$$f_{\sigma i}^{(0)} = A_{\sigma i}(\rho) + B_{\sigma i}(\rho)\mathbf{e}_{\sigma i}\cdot\mathbf{u} + C_{\sigma i}(\rho)(\mathbf{e}_{\sigma i}\cdot\mathbf{u})^2 + D(\rho)_{\sigma i}\mathbf{u}^2 \tag{7}$$

A Chapman-Enskog procedure is then applied to determine the macroscopic behavior of this model. The values of $A_{\sigma i}$, $B_{\sigma i}$, $C_{\sigma i}$ and $D_{\sigma i}$ are chosen so that the macroscopic behavior matches the Navier-Stokes equations to as high an order as possible. The resulting continuity and momentum equations follow.

$$\frac{\partial\rho}{\partial t} + \frac{\partial\rho u_\beta}{\partial x_\beta} + O(\varepsilon^2) = 0 \tag{8}$$

$$\rho\frac{\partial u_\alpha}{\partial t} + \rho u_\beta\frac{\partial u_\alpha}{\partial x_\beta} = -\frac{\partial p}{\partial x_\alpha} + \frac{\partial}{\partial x_\beta}\left(\mu\left(\frac{\partial u_\beta}{\partial x_\alpha} + \frac{\partial u_\alpha}{\partial x_\beta}\right)\right) + O(\varepsilon^2) + O(M_\alpha^3) \tag{9}$$

Characteristic dimensionless parameters are the Mach number, $M_a = \sqrt{3}U/c$ where U is a characteristic macroscopic flow speed and $c = 1$ in lattice units, the Knudsen number which is proportional to $\varepsilon = c\tau/L$ where L is a macroscopic flow length, and the Reynolds number, $Re = \rho UL/\mu$.

2.2. TRIANGULAR (FHP) LATTICE MODEL

Another lattice model commonly used in two-dimensional LB simulation is a triangular lattice (FHP) model. There are two types of particles on each node of the FHP model: rest particles and moving particles with unit velocity $\mathbf{e}_i$ along six directions as shown in Fig.2. The equilibrium distributions for the FHP model are given as,

$$f_0^{(0)} = d_0 - \rho\mathbf{u}^2 = \rho\alpha - \rho\mathbf{u}^2 \tag{10}$$

$$f_i^{(0)} = d + \frac{1}{3}\rho\left[(\mathbf{e}_i \cdot \mathbf{u}) + 2(\mathbf{e}_i \cdot \mathbf{u})^2 - \frac{1}{2}\mathbf{u}^2\right]$$
$$= \frac{\rho - \rho\alpha}{6} + \frac{1}{3}\rho\left[(\mathbf{e}_i \cdot \mathbf{u}) + 2(\mathbf{e}_i \cdot \mathbf{u})^2 - \frac{1}{2}\mathbf{u}^2\right] \tag{11}$$

where α is an adjustable parameter. If the ratio of rest and moving particles is defined as $\lambda = d_0/d$, the pressure is determined by the isothermal equation of state,

$$p = 3d = \frac{(1-\alpha)\rho}{2} = \frac{3}{\lambda + 6}\rho \tag{12}$$

and the speed of sound is

$$c_s^2 = \frac{1-\alpha}{2} = \frac{3}{\lambda + 6} \tag{13}$$

The viscosity is related to the relaxation time through an equation of the form

$$\nu = \frac{2\tau - 1}{8} \tag{14}$$

2.3. CUBIC LATTICE MODEL

A cubic lattice[17] with unit spacing is used on which each node has fourteen nearest neighbors connected by fourteen links. Particles can only reside on the nodes and move to their nearest neighbors along these links in the unit time as shown in Fig.3. Hence, there are two types of moving particles. Particles of type 1 move along the axes with speed $|\mathbf{e}_{1,i}| = 1$ and particle of type 2 move along the links to the corners with speed $|\mathbf{e}_{2,i}| = \sqrt{3}$. Rest particles with speed zero are also allowed at each node.

A suitable equilibrium distribution can be chosen in the following form for particles of each type

$$f_{01}^{(0)} = \rho\alpha - \frac{2}{3}\rho\mathbf{u}^2 \tag{15}$$

$$f_{1i}^{(0)} = \rho\beta + \frac{1}{3}\rho(\mathbf{e}_{1i} \cdot \mathbf{u}) + \frac{1}{2}\rho(\mathbf{e}_{1i} \cdot \mathbf{u})^2 - \frac{1}{6}\rho\mathbf{u}^2 \tag{16}$$

$$f_{2i}^{(0)} = \rho\frac{(1 - 4\beta - \alpha)}{4} + \frac{1}{12}\rho(\mathbf{e}_{2i} \cdot \mathbf{u}) + \frac{1}{8}\rho(\mathbf{e}_{2i} \cdot \mathbf{u})^2 - \frac{1}{24}\rho\mathbf{u}^2 \tag{17}$$

Values of $\alpha = 2/9$ and $\beta = 1/9$ are used. The relaxation time is related to the viscosity by

$$\tau = \frac{6\nu + 1}{2} \tag{18}$$

where ν is the kinematic viscosity measured in lattice units.

3. Two-dimensional Homogeneous Isotropic Turbulence

3.1. INITIAL AND BOUNDARY CONDITIONS

The initial condition of the vorticity is randomly determined by satisfying the relation,

$$E(k) = \frac{1}{2} \sum_{|k'-k| \leq 1/2} | \tilde{\omega}(k_1, k_2) |^2 / k'^2 = \frac{2}{3} k \exp\left(-\frac{2}{3}k\right) \qquad (19)$$

where ω denotes the vorticity in the Fourier space, $k'^2 = k_1^2 + k_2^2$, and k_1 and k_2 are the wave numbers. The periodic boundary conditions are imposed in the x and y directions. The computational domain is square, $(0,0) \leq (x,y) < (2\pi, 2\pi)$.

3.2. LOW REYNOLDS NUMBER SIMULATION

In order to compare the results of the LBGK method with those of the MOL, numerical simulation using the square lattice model is carried out for a low Reynolds number. The kinematic viscosity is chosen as $\nu = 0.01$. The number of lattice nodes is 129×129 (129 lattice nodes and 128 lattice units in one side). In this case, the initial integral scale Reynolds number R_L corresponds to $R_L = 31.9$, which is expressed as $R_L = \Omega/\nu\eta^{\frac{1}{3}}$. Ω and η denote the total energy and the enstrophy dissipation rate, which are defined as

$$\Omega = \int_0^\infty E(k)dk, \quad \eta = 2\nu \int_0^\infty k^4 E(k)dk \qquad (20)$$

Perhaps the most striking verification of the accuracy of the LBGK method is found in the direct comparison of contour plots of vorticity between the LBGK method and higher-order MOL at the same physical time. Fig.4 displays comparison of vorticity contours at $t = 2.0$ between the square lattice BGK method (solid line) and 10th-order MOL (dashed line). The vorticity distribution is extremely similar down to detailed structure in the two simulations. Simulation by using the triangular (FHP) lattice BGK method is also performed for the same initial condition on lattice nodes. In Fig.5 comparison of vorticity contour plots at is shown between the square lattice (solid line) and the FHP lattice (dashed line). Once again, the plots from the two methods show excellent agreement. In order to investigate the behavior of statistical quantities, time history of (a) the total energy Ω, (b) the enstrophy Q and (c) the enstrophy dissipation rate η is shown in Fig.6, where the enstrophy Q is defined as $Q = \int_0^\infty k^2 E(k)dk$. Here Ω and Q are inviscid invariants, and therefore are monotonically decreasing in this dissipative simulation. The solid line, dotted line, and dashed line indicate to these quantities for the square lattice model, FHP lattice model, and

10th-order MOL, respectively. What is evident in Fig.6 is that the LBGK method tracks the higher-order MOL closely with respect to evolutions of Ω, Q and η. Wave number spectra of the total energy are also compared in Fig.7 which clearly displays the excellent match between the three methods. In the simulation of low Reynolds number case, no significant difference is observed between the square and triangular lattice models for this resolution.

3.3. HIGH REYNOLDS NUMBER SIMULATION

As a large-scale direct numerical simulation of high Reynolds number homogeneous isotropic turbulence, simulation for the case with $\nu = 0.0001$ is carried out. This corresponds to the initial integral scale Reynolds number $R_L = 25500$. The number of lattice nodes is 1025×1025. Fig.8 shows comparison of vorticity contour plots at $t = 3.0$ between the square lattice BGK method and the 10th-order MOL. Although slight difference in vorticity contours is noticeable at late time, strikingly similar features can be found for the LBGK simulation, as compared with the solutions by the 10th-order MOL.

Time history of (a) the total energy Ω and (b) the enstrophy dissipation rate η is shown in Fig.9. Since Reynolds number is much higher than the previous case, decrease in Ω is much less than observed in Fig.6(a). In contrast to Ω and Q which are monotonically decreasing in these cases, η can be amplified, as much as dissipated, and not monotonic as shown in Fig.9(b). Wave number spectra of $k^3E(k)$ at $t = 3.0$ are compared in Fig.10. From this figure it is seen that two methods yield quite a similar answer in terms of the statistical behavior of the flow. With the present lattice of 1025×1025 nodes, the inertial range of two-dimensional turbulence can be resolved. The spectrum shown in Fig.10 indicates that there is a range of wave number $k \leq 50$ for which $k^3E(k)$ is roughly constant so that $E(k)$ is proportional to k^{-3}.

Computational cost of the LBGK method for this high Reynolds number simulation on SGI POWER ONYX 10000 is compared in table 1 with that of the 10th-order MOL. As far as efficiency is concerned, the LBGK method requires less than half CPU time per characteristic time of that of the MOL.

4. Three-dimensional Homogeneous Isotropic Turbulence

4.1. INITIAL AND BOUNDARY CONDITIONS

Three-dimensional decaying turbulence is simulated with a random initial condition having the energy spectrum;

$$E(k) = 16\sqrt{2/\pi}\nu_0^2 k_{max}^{-5} k^4 \exp\left[-2(k/k_{max})^2\right] \tag{21}$$

where we set $\nu_0 = 1.0$ and the peak wave number $k_{max} = 4.75683$ for low Reynolds number case and $k_{max} = 2.37841$ for medium Reynolds number one. The periodic boundary conditions are imposed in the x, y and z directions. The computational domain is a cube, $0 \leq (x, y, z) \leq 2\pi$.

4.2. LOW AND MEDIUM REYNOLDS NUMBER SIMULATIONS

Numerical simulations are carried out for two cases. In the first case the kinematic viscosity is chosen as $\nu = 0.01189$. The initial integral scale and micro scale Reynolds number is $30 \sim 45$ which corresponds to low Reynolds number simulation. In the medium Reynolds number case $\nu = 0.0025$ is chosen which corresponds the initial integral scale and micro scale Reynolds number=340. The number of lattice nodes is $65 \times 65 \times 65$.

Contour surface of the enstrophy at $t = 0.5$ for the cubic LBGK method and the MOL for $\nu = 0.01189$ are shown in Fig.11(a) and (b) respectively. The enstrophy Ω is defined as

$$\Omega(x, y, z) = \frac{1}{2}(\omega_x^2 + \omega_y^2 + \omega_z^2) \tag{22}$$

Plot value is $\Omega_{plot} = 150$. Contour surface of the enstrophy computed by two methods are almost indistinguishable. Time history of the total energy and the enstrophy for medium Reynolds number are compared in Fig.12(a) and (b). The former is monotorically decreasing while the latter is amplified. Wave number dependence of energy spectrum $E(k)$ at $t = 0.7$ is also compared in Fig.13. From these figures it is seen that two methods yield quite a similar results in terms of the statistical behavior of the flow. Computational cost of the LBGK method for low Reynolds number simulation on a SGI POWER ONYX 10000 is also compared in Table 1 with that of the 10th-order MOL. As far as efficiency is concerned, the LBGK method requires 26% less CPU time than that of the MOL. Comparison between the cubic LBGK method and the MOL shows that the cubic LBGK method can be an alternative for solving the Navier-Stokes equations.

5. Conclusions

Two- and three-dimensional simulations of decaying homogeneous isotropic turbulence using the LBGK method have shown that the method is as accurate as the conventional method using the same lattice size. The LBGK method is able to reproduce the dynamic of decaying turbulence and could be an alternative for solving the Navier-Stokes equations. Further investigation is needed on the accuracy and efficiency of cubic LBGK model.

References

1. J.R.Herring, S.A.Orszag, R.H.Kraichman, and D.G.Fox, J. Fluid Mech., 66, (1974) 417.
2. D.GFox, and S.A.Orszag, L. Comp. Phys., 11, (1973) 612.
3. B.Fornberg, 1997, J. Comp. Phys., 25, (1997) 1.
4. N.Satofuka and H.Nishida, BAIL III, Boole Press, (1984), 291.
5. N.Satofuka and H.Nakamura and H.Nishida, Lecture Notes in Physics 218, Springer-Verlag, Berlin, (1984), 475.
6. H.Nishida and N.Satofuka, International Journal for Numerical Method in Engineering 34, (1992) 637.
7. H.Nishida and N.Satofuka, Finite Elements in Analysis and Design 16 (1994) 285.
8. U.Frisch, B.Hasslacher and Y.Pomeau. Phys. Rev. Lett. 56, (1986) 1505.
9. G.McNamara and G.Zanetti, Phys. Rev. Lett. 61, (1988) 2332.
10. F.Higuera and J.Jimenez, Europhys, Lett. 9, (1989) 663.
11. F.Higuera and S.Succi, Europhys, Lett. 8, (1989) 517.
12. S.Chen, H.Chen, D.Martinez, and W.H.Matthaeus. Phys. Rev. Lett. 67, (1991) 3776.
13. H.Chen, S.Chen, and W.H.Matthaeus, Phys. Rev. A 45, (1992) 5539.
14. Y.Qian, Ph.D. thesis. de I'Universit e Pierre et Marie Curie. January 1990.
15. Y.Qian, D.d'Humieres, and P. Lallemand, Europhys. Lett. 17(6), (1992) 479.
16. P.L.Bhatnagar, E.P.Gross, and M.Krook. Phys. Rev. 94, (1954) 511.
17. S.Hou, Q.Zou, S.Chen, G.Doolen, and A.C.Cogley. Journal of computational physics. 118, (1995) 329.
18. N.Satofuka, in: Numerical Properties and Methodologies in Heat Transfer, edited by T.M.Shin, Hemisphere, Washington, DC, (1983) 97.

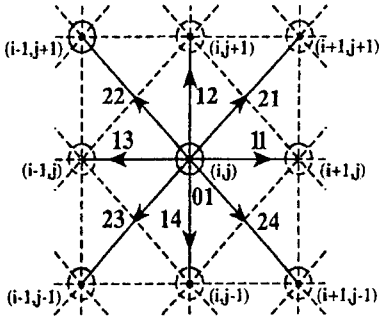

Figure 1. Square lattice model

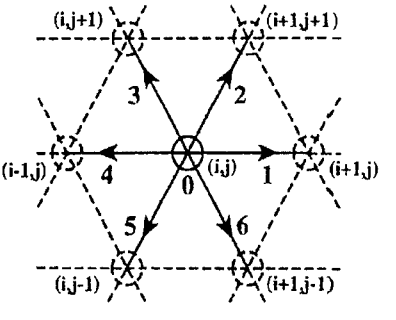

Figure 2. Triangular lattice model

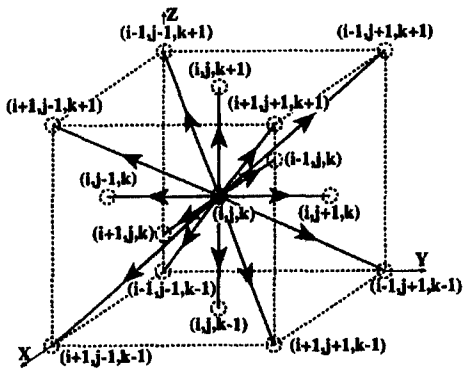

Figure 3. Cubic lattice model

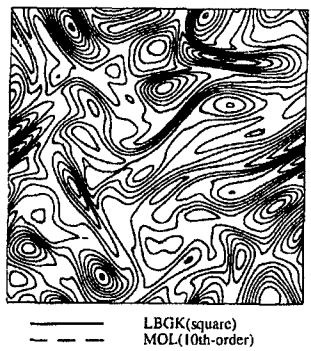

Figure 4. Comparison of vorticity countours between LBGK(square) and MOL(10th-order) at $t = 2.0$, $\nu = 0.01$

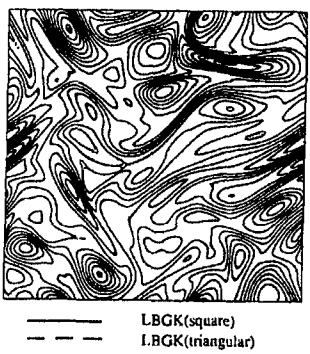

Figure 5. Comparison of vorticity countours between LBGK(square) and LBGK(triangular) at $t = 2.0$, $\nu = 0.01$

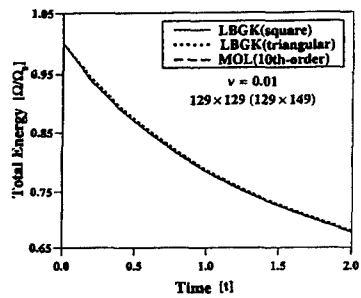

Figure 6(a). Time history of total energy Ω computed by LBGK(square), LBGK(triangular) and MOL(10th-order) for $\nu = 0.01$

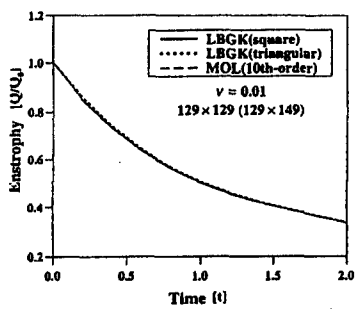

Figure 6(b). Time history of enstrophy Q computed by LBGK(square), LBGK(triangular) and MOL(10th-order) for $\nu = 0.01$

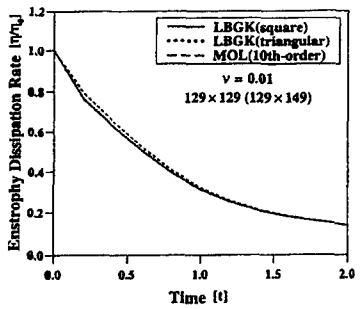

Figure 6(c). Time history of enstrophy disspation rate η computed by LBGK(square), LBGK(triangular) and MOL(10th-order) for $\nu = 0.01$

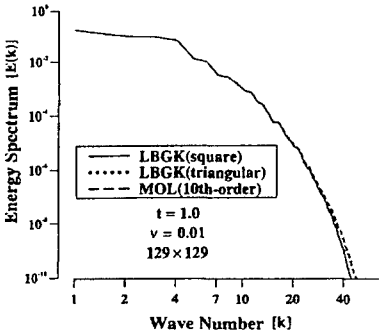

Figure 7. Wave number dependence of energy spectrum $E(k)$ computed by LBGK(square), LBGK(triangular) and MOL(10th-order) at $t = 1.0$, $\nu = 0.01$

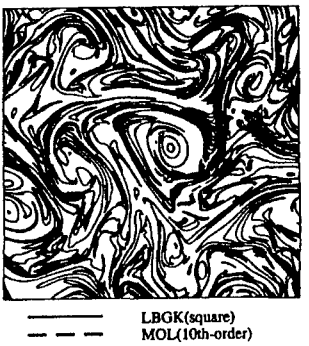

Figure 8. Comparison of vorticity countours between LBGK(square) and MOL(10th-order) at $t = 3.0$, $\nu = 0.0001$

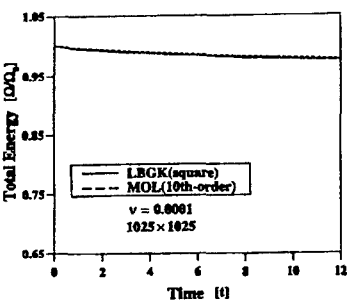

Figure 9(a). Time history of total energy Ω computed by LBGK(square) and MOL(10th-order) for $\nu = 0.001$

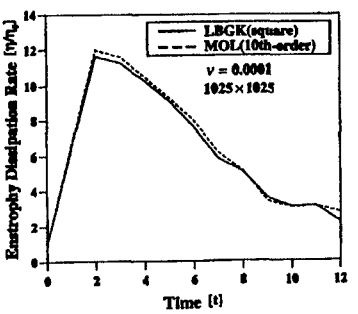

Figure 9(b). Time history of energy dissipation rate η computed by LBGK(square) and MOL(10th-order) for $\nu = 0.001$

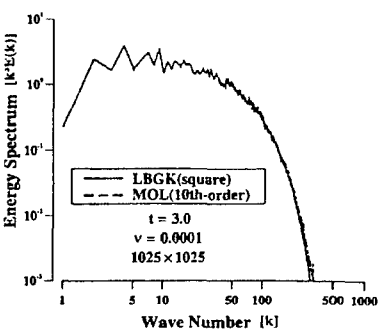

Figure 10. Wave number dependence of energy spectrum $k^3E(k)$ computed by LBGK(square) and MOL(10th-order) at $t = 3.0$, $\nu = 0.0001$

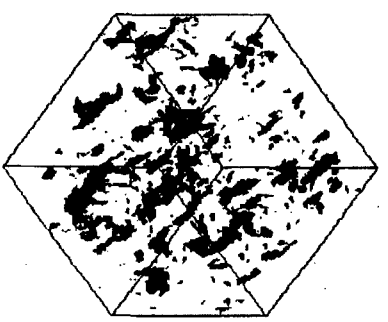

Figure 11(a). Enstorophy contours at $t = 0.5$ for the cubic LBGK method

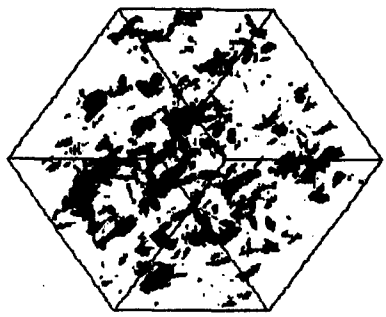

Figure 11(b). Enstorophy contours at $t = 0.5$ for the MOL

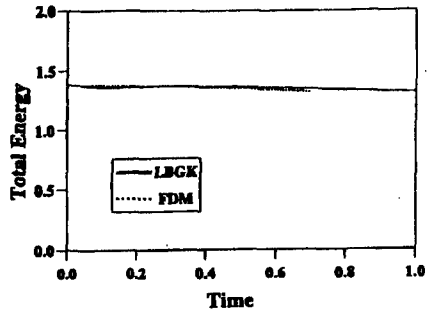

Figure 12(a). Time history of total energy computed by LBGK(cubic) and MOL for $\nu = 0.0025$

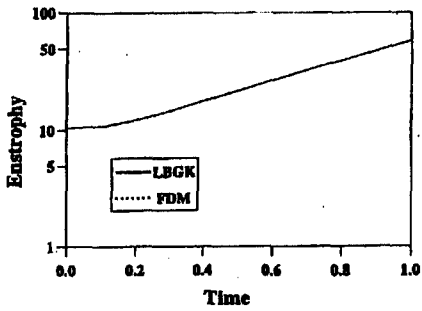

Figure 12(b). Time history of enstrophy computed by LBGK(cubic) and MOL for $\nu = 0.0025$

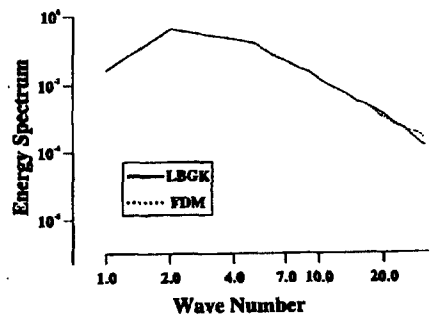

Figure 13. Wave number dependence of spectrum $E(k)$ at $t = 0.7$

TABLE 1. Comparison of computational cost

two-dimension		three-dimension	
LBGK(square)	MOL(10th-order)	LBGK(square)	MOL(10th-order)
$\sqrt{\langle u^2 \rangle} = 0.04$	$\Delta t = 0.001$	$\sqrt{\langle u^2 \rangle} = 0.01$	$\Delta t = 0.01$
4047[time step]	1000[time step]	1019[time step]	100[time step]
$t = 1.0$	$t = 1.0$	$t = 1.0$	$t = 1.0$
63006 < 1 >	136639 < 2.17 >	8686[sec] < 1 >	10924[sec] < 1.26 >
15.47[sec/time step] < 1 >	136.64[sec/time step] < 8.83 >	8.52[sec/time step] < 1 >	109.24[sec/time step] < 12.82 >